Paper # 3

Influence of Silica Characteristics on Tire Performance Indicators

By Wilma K. Dierkes[1], Ernest Cichomski, E.C.[1], Tanya Tolpekina[2], Steven Schultz[2], Anke Blume[1] and J.W.M. Noordermeer[1]

[1]University of Twente, Engineering Technology, Elastomer Technology & Engineering, Enschede, Netherlands

[2]Apollo Tyres Global R&D B.V., Enschede, Netherlands

Presented at the Fall 186th Technical Meeting of
Rubber Division, ACS
Nashville, TN
October 14-16, 2014

ISSN:

* Speaker

ABSTRACT

In this study, five different rubber reinforcing silica types are investigated concerning their influence on properties related to tire performance. The silicas are characterized by different specific surface areas, aggregate sizes and structure, but with otherwise comparable properties. A standard “Green tire” tread recipe is used as base compound, and bis-(triethoxysilylpropyl)tetrasulfide (TESPT) is used as coupling agent. The amount of coupling agent is adjusted to the specific CTAB surface area of the silicas. The silicas are tested in two modes: the silica loading is kept constant and the silica loading is empirically adjusted to reach equal hardness in the vulcanized state. The value of the dynamic loss tangent, tan δ at 60 °C is used to assess the influence on rolling resistance, and the Laboratory Abrasion Tester (LAT 100) is used to evaluate the wet skid resistance of the tested compounds. This equipment was chosen due to the good correlation with on-road tests. Besides these tire performance indicators, also other properties are investigated in this paper. Silica with the smallest aggregate size provides superior wet skid resistance at constant loading mode. The highest wet skid resistance is maintained even when the silica load is decreased to equalize the hardness of its corresponding vulcanizates. A decreased concentration of the high surface area silica provides also low values of tan δ at 60 °C which correspond with better rolling resistance of tires made therewith.

INTRODUCTION

Despite many studies on the performance of tire tread compounds, thorough knowledge of the influence of the characteristics of silica reinforcing fillers on wet skid and rolling resistance is still limited. It is well-known that by the change from carbon black to a silica-silane filler as reinforcing system, the rolling and wet skid resistances of tire treads are improved. Therefore, the

present European passenger car tire industry uses preferably silica as filler in tire tread formulations. Apart from the rolling resistance improvement, the wet skid or traction performance of tire treads is also an important safety and performance criterion. However, it is still somewhat questionable which silica characteristics result in a simultaneous improvement of wet skid resistance as well as rolling resistance. The friction, traction or skid resistance, in dry and wet conditions, of tire treads on various surfaces has been subject of numerous experimental and modeling studies already: Wang [1,2,3], Heinz and Grosch [4,5,6], Derham [7], Heinrich et al. [8,9,10], Klüppel and Heinrich [11], Müller et al. [12], Le Gal and Klüppel [13], Persson et al. [14], Isono et al. [15].

In order to investigate the influence of the specific silica surface area, aggregate size and structure on tire performance indicators, five different highly dispersible silica types are compared in the present study. Commercially available silicas can be divided into two groups: conventional silicas (CV) and highly dispersible silicas (HDS). U.S. Patent No. 6,180,076 discloses HDS defined by the ratio of the peak heights of primary particles in non-degraded state (1-100 μm) to their size in degraded state (< 1 μm), that is after ultrasonic treatment, termed the Wk coefficient. In HDS this coefficient must not exceed a level of 3.4 and the lower the value, the higher is the silica dispersion level [16,17]. The major difference between conventional silica and HDS lays in their structure and aggregate size distribution. Aggregates of HDS are more branched, with 3-4 branches on average. This results in the fact that HDS has an improved dispersion over the conventional ones due to better transfer of shear forces during mixing [18,19]. The aggregate size distribution for both conventional and HDS is shown in FIG. 1.

The specific surface areas measured in accordance with Brunauer Emmett Teller (BET) and Cetyl Trimethylammonium Bromide (CTAB) describe the accessibility of the silica surface to relatively small molecules like nitrogen in case of the BET measurement, or relatively large

molecules like polymers in the case of the CTAB measurements [20,21]. The BET value is a measure of the "total" surface area, while the CTAB value corresponds to the "outer" surface area of the silica. The ratio of BET to CTAB is often used to compare the particular silica types. A large difference between the two specific surface areas is hard to achieve. For the majority of silica types the value of the BET to CTAB ratio ranges somewhere in between 0.8 and 1.2. However higher values of 1.5 to 2.4 are also reported in the literature [22,23,24].

The goal of the present study is to characterize the underlying mechanisms involved in filler-rubber interactions for wet skid and rolling resistance of tire treads, a dynamic-viscoelastic phenomenon. The storage and loss moduli are commonly measured as dynamic properties for the assessment of the tire properties. The ratio of loss to storage modulus is the definition of the loss tangent or tangent delta. The influence of the filler-polymer interaction on wet skid performance is investigated by testing the dynamic properties, the tan δ in the temperature range from 0 – 20 °C at 10 Hz. The values of the loss angle in this temperature range are so far considered to be the most suitable indicators for the wet skid performance of a tire tread [8,25,26]. Assessment of rolling resistance by measuring the tangent delta value at 40 – 60 °C on laboratory scale is common practice, and a correlation between dynamic properties of the material and on-road tests is widely accepted [27]. Additionally, measurements on a Laboratory Abrasion Tester 100 (LAT 100) are performed to assess the wet skid performance, as this method comes closer to the practical case of a rolling tire [28,29].

EXPERIMENTAL

MATERIALS AND COMPOUND FORMULATIONS

To assess the influence of the silica specific surface area and morphology on the wet skid, rolling resistance and other related properties, 5 types of silica differing in these two properties but otherwise comparable were used in this study. The silica samples are commercial grades produced by Rhodia Silices, presently member of the Solvay group (Lyon, France). The physical properties of these silica types are described in Table I. A detailed specification of the other compounding ingredients is shown in Table II. Particular attention is drawn to two silica types, namely Zeosil 200MP and Zeosil 1200 MP. Measurements of the BET specific surface area gives evidence of similar primary particle size of these two silicas. However the aggregate size measurements performed after the desagglomeration confirm existence of the larger aggregates for Zeosil 200MP. Considering the dimensions given by these two experiments, a model depicting the morphology of these two silicas can be drawn, see FIG. 2. The model shows also a different aspect ratio of these two silica types.

Bis-(triethoxysilylpropyl)tetrasulfide (TESPT) was chosen as coupling agent. The experiments were performed using a typical "Green tire" recipe as given in Table III and Table IV [30]. The TESPT content was adjusted to the surface area of the particular silica type by using the empirical equation proposed by L. Guy et al. [31] (Equation 1).

$$TESPT\ (phr) = 5.3\times10^{-4} \times (CTAB)_{silica} \times (phr)_{silica} \qquad \text{(Equation 1)}$$

Two series of batches were prepared:

Series I, in which the silica loading was kept at the same level of 80 phr (Table III).

Series II, in which the silica loading was empirically adjusted to obtain equal hardness for all compounds after vulcanization (Table IV). Similar hardness of the samples provides more comparable materials for the LAT 100 tests.

MIXING AND VULCANIZATION

A 1.6 liter Banbury mixer was used for mixing. This process was done in three steps according to the parameters as given in Table V. The first two steps of the mixing process were done in the internal mixer with an initial set temperature of 40 °C. The dump temperature of the compound was adjusted to be 155 °C by manually changing the cooling water flow and changing the rotor speed, if necessary. Addition of curatives was done on a two roll mill preheated to 50 °C.

Vulcanization of the sheeted samples for tensile tests was performed on a Wickert laboratory press (WLP 1600) at 160 °C and 100 bar for an optimal curing time (t_{95}) obtained from Moving Die Rheometer (MDR 2000, Alpha Technologies) measurements according to ISO 6502. The samples for hardness tests were prepared in cylindrical molds and cured for a period of two times the t_{90}. The samples for the DIN abrasion test were cured for t_{90} multiplied by 1.2. The adjustment of the curing time as measured in the rheometer was necessary due to the high thickness of the samples and the low thermal conductivity of the rubber compounds.

CHARACTERIZATIONS METHODS

The Mooney viscosity ML(1+4) of the compounds was measured at 100 °C on a Mooney viscometer MV2000E (Alpha Technologies) according to ISO 289-1.

Payne effect measurements were done by using a Rubber Process Analyzer, RPA 2000 from Alpha Technologies, after prior vulcanization for 1.2 x t_{90} at 160 °C in the RPA 2000. In order to assess the Payne effect values, the storage moduli at 1% strain and 90% strain were measured at 100°C and a frequency of 0.5 Hz.

Mechanical properties of the samples were tested using a Zwick Z020 tensile tester according to ISO-37. A crosshead speed of 500 mm/min was used. The measurements were done at ambient temperature.

Filler macrodispersion measurements were done using the visual microscopic inspection method with 100 × magnification according to ISO 11345 method C. Measurements were done by using a Leica microscope.

Shore A hardness of the samples was measured in five different places on the samples, which were cylindrical with a diameter of 10 mm. The median value was given as a representative hardness of the particular sample.

Abrasion resistance was measured by a DIN abrader machine (Abrasion tester 564C from Karl Frank GmbH) according to method A of DIN 53516. The weight loss was measured and recalculated to a volume loss for each sample.

In order to characterize the wet skid resistance, dynamic mechanical analysis was performed on a Gabo Dynamic Mechanical Analyzer in a temperature-sweep mode from -100 °C to +100 °C with 1 % static and 0,1 % dynamic strain and a frequency of 10 Hz. In order to predict the rolling resistance, single point measurements of tan δ (= G”/G’) at 60 °C with 2 % strain and a frequency of 10 Hz were made, where G’ is the storage modulus and G” the loss modulus.

A Laboratory Abrasion Tester 100 (LAT 100, VMI the Netherlands) was used to estimate the wet skid resistance of the tire treads in conditions which simulate the real conditions on a road: FIG. 3 [4]. Wheel samples were made by compression molding in a special mold using the Wickert laboratory vulcanization press for 11 mins. at 170 °C. Testing was performed at five different water temperatures: 2 °C, 8 °C, 15 °C, 22 °C, 30 °C and at constant slip angle of 15°. An electro-corundum disc with relative roughness 180 was used to simulate the tire-road interactions. Tests were performed at constant speed of 1,5 km/h and load of 75 N for a distance of 33 meters. The Side Force Coefficient (SFC) values (Equation 2) for the particular samples are compared with the value obtained for the reference sample and given as relative values. The property with higher rating is always better.

$$SFC = \frac{F_y}{F_z} \quad \text{(Equation 2)}$$

Where F_y = the side force; and F_z = the normal load on the rubber wheel sample.

RESULTS AND DISCUSSION

MIXING FINGERPRINTS

The energy consumption during mixing is an important factor from both an economic and environmental point of view. Power profile and mixing chamber temperature were registered and are shown in FIG. 4 and FIG. 5 for the first mixing stage, as well as FIG. 6 and FIG. 7 for the second mixing stage. As the silicas are characterized by different specific surface areas, the degree of filler-polymer interaction varied, and thus the shear forces during mixing differed in strength. Hence, to prevent an excessive rise in the discharge temperature the mixing time had to be shortened for some batches.

The second mixing stage was preceded by 24 hours of batch stabilization. With increasing surface area, the mixing process became more energy consuming, caused by the fact that with the same amount of silica (80 phr), different total surface areas are involved in the mixing process.

Fingerprints of the first mixing stage for Series II, which contain variable amounts of silica, are shown in FIG. 8 and FIG. 9. In order to obtain equal hardness, the silica loading was increased for the low reinforcing types, SSA-80 and SSA-110 and decreased for the highly reinforcing types, SSA-195 and SSA-200. The value of hardness obtained for the batch containing 80 phr of silica SSA-160 was used as reference value. Increase of the silica loading with lower reinforcing capabilities, lower specific surface area, still turns out to result in higher shear forces: FIG. 8. This points at the benefit of using a relatively small amount of highly reinforcing fillers over larger amounts of low reinforcing fillers. By the strong reinforcing effect caused by silicas with

smallest aggregates and highest specific surface area, the loading of the silicas can in fact be decreased resulting in lower energy consumption during mixing.

The second stage of mixing is shown in FIG. 10 and FIG. 11. Again, it shows that the batch containing 65 phr of silica SSA-195, the highly reinforcing type, is characterized by the lowest energy consumption.

COMPOUND MOONEY VISCOSITY

The Mooney viscosity of the compounds increases substantially with increasing CTAB surface area of the silicas as shown in FIG. 12. An increased surface area of the silica is the result of a smaller size of the primary particles (Table), and both properties tend to increase the viscosity: smaller particles result in lower inter-particle distances for a given degree of dispersion. Thus these particles have a higher mutual interaction and higher forces are need to displace the particles within the elastomer matrix. Furthermore, a higher surface area increases the filler-polymer interaction, which results in a higher degree of rubber immobilized on the surface of the filler. This increases the effective diameter of the filler, which also results in an increase of the viscosity.

The Mooney viscosity for SSA-200 in Series I is 4 MU lower in comparison to the SSA-195. However, considering the specific surface area of SSA-200, the viscosity of the compound containing this filler should be higher or at the same level as for SSA-195. The off-trend viscosity for silica SSA-200 is even more pronounced when the Mooney viscosity is plotted against the aggregate size; see FIG. 13. This discrepancy in viscosity can be caused by the different aggregate morphology of silica SSA-200. The aggregates of silica SSA-200 are substantially larger than those of the SSA-195 at comparable specific surface areas.

Filler agglomerates are broken and dispersed in the rubber by mechanical mixing. The more branched structure of silica SSA-200 shown in FIG. 2 facilitates transfer of shear forces during

mixing. Therefore, a more effective disagglomeration and better dispersion are obtained for the compounds containing SSA-200 in comparison with the silica SSA-195: see FIG. 14.

TENSILE PROPERTIES

The tensile strength gives information about the strength of interactions between filler particles and polymer chains at high deformation. An extreme example of this effect is when the compound is filled with silica without using a coupling agent. When filler-polymer interaction is low, the polymer chains adsorbed or entangled on the filler surface slide on the filler surface under the influence of the applied load and are desorbed from the filler surface. Molecular slippage of chains on the filler surface is also known for carbon black filled elastomers [32,33]. At medium strain, the load is transferred via polymer entanglements, and finally, when all entanglements are disentangled, the load is transferred via the crosslinked polymer chains [34,35]. In such a case the fillers show a relatively low reinforcing effect: tensile strength is low and elongation at break is high. When the polymer chains are linked to the filler surface via covalent bonds, for instance by a coupling agent, the elongation at break drops but the tensile strength increase, because the molecular slippage phenomena are suppressed.

Along with the increasing CTAB surface area, the tensile strength of the vulcanized compounds rises. The tensile strength value for the SSA-200 is only slightly lower in comparison to the SSA-195, as seen in FIG. 15.

When the tensile strength is plotted versus aggregate size: FIG. 16, it decreases with increasing aggregate size. Now the tensile strength of the SSA-200 is following the general trend. Apparently the aggregate size is the governing factor to influence the tensile strength. It should be emphasized that the aggregate size does not necessarily correlate with the primary particle size. The aggregates of silica SSA-200 are much larger than the aggregates of SSA-195.

However, the minor differences in the specific surface areas of these two silicas suggest that their primary particle sizes must be similar.

For the series of batches in which the silica loading was adjusted to keep the hardness at constant level, the tensile strength depends only slightly on the aggregate size or specific surface area. Apart from silica loading, the tensile strength of the vulcanizates therefore depends mainly on the aggregate size which determines the reinforcing capabilities of the fillers.

The elongation at break is shown in FIG. 17 and FIG. 18. The general trend becomes also more clear now: along with increasing surface area of the silica or decreasing aggregate size, elongation at break increases. The value of the elongation at break is more sensitive to the filler structure than the tensile strength.

Just like in Series-I, the general trend of increasing elongation at break with decreasing aggregate size is also visible for the series with equal hardness, Series-II. Despite the fact that the silica loading is adjusted, still the aggregate size has a dominating effect on elongation at break. Taking into the consideration that the filler-filler interactions measured with the Payne effect for the Series-II are similar, see below in FIG. 19, the polymer-filler interactions must differ for each silica type. The more polymer is adsorbed at the filler surface by the smaller aggregate size the higher elongation at break can be reached.

The ability of crack dissipation or propagation has also an impact on elongation at break. At the final stages of straining, cracks are formed somewhere in the rubber sample, which lead to sample damage. Samples, in which cracks can propagate easily throughout the body of the sample, have lower values of elongation at break. It seems that highly reinforcing fillers can dissipate cracks more efficiently, resulting in a higher elongation at break.

FILLER-FILLER INTERACTIONS – PAYNE EFFECT

The Payne effect [36] may be used as an indication for filler-filler interaction; it is an indirect method that allows to assess the interactions, partly also due to the dispersion of the filler in a polymer matrix. It is measured as the difference between the storage modulus measured at low and high strain. Physically, it can by described as the difference between two different states of the filler-rubber composite: one state in which the filler network dominates in the composite, and energy can be transferred through this filler network; and a second state in which the silica network is broken and energy must be absorbed by the matrix.

Decreasing specific surface area of the silica or larger particles lead to a reduced Payne effect: FIG. 19, due to a less developed filler-filler network. Where the silicas SSA-80 and SSA-110 are characterized by low Payne effects, their value as reinforcing filler is also lower: FIG. 16.

Again, aggregate size is a more appropriate parameter to plot the Payne effect than CTAB specific surface area, as shown in FIG. 19 and FIG. 20. It is well known that smaller particle fillers are more difficult to disperse because of the higher particle to particle affinity. Adjustment of the silica loading in order to equalize the Shore A hardness: Series II, causes also more or less equal values of the Payne effect for all samples.

HARDNESS

In general, hardness of vulcanizates can be correlated with filler-filler interactions and silica loading. For instance, in the extreme case of no coupling agent, thus low filler-polymer and high filler-filler interactions, much higher hardness values are observed. Introduction of coupling agent suppresses the filler-filler interactions and consequently reduces the hardness.

With increasing dimensions of the silica aggregates, the hardness of the vulcanizates decreases: FIG. 21, Series-I. Adjustment of the silica loading in Series-II causes equalization of the filler-filler interactions as well, see FIG. 20.

ABRASION RESISTANCE

It is commonly accepted that there is inverse relation between the glass transition temperature of a polymer matrix and abrasion resistance. DIN abrasion is expressed in volume loss, and describes the ability of the rubber composite to resist tearing-off small pieces of rubber from its surface by the sharp asperities of the counter surface. When the same formulation is used, the abrasion represents the strength of polymer-filler interactions: the stronger the interaction, the more difficult it is to break small particles out of the rubber composite. Abrasion resistance turns out to be worse for larger aggregate size, as shown in FIG. 22.

The fact that smaller aggregate sizes result in higher abrasion resistance may be related again to better interaction with the polymer due to the higher available contact area. The degree of dispersion might be lower for the finer silica types, but this effect is not strong enough to counterbalance the effect of the strong filler-polymer interaction. Silica's with a smaller aggregate size, for example SSA-160, SSA-200 and SSA-195, are therefore the preferred fillers in terms of abrasive wear resistance.

The compounds in which the silica loading was adjusted to equalize the hardness show a more comparable abrasion loss than without adjustment, but the general trend is not changed. Moreover, the abrasion losses obtained for the compounds containing highly reinforcing silicas like SSA-160, SSA-200 and SSA-195 are less affected than for low reinforcing types. In all cases, except for the sample with silica SSA-195, equalizing the hardness improves the abrasion resistance.

DYNAMIC MECHANICAL ANALYSIS

In general two effects related to the tan δ curve are visible in FIG. 23:

1. The tan δ peak becomes broader and shifts towards a higher temperature with decreasing silica aggregate size. This effect is visible just for Series-I;
2. The height of the tan δ peak drops with decreasing aggregate size. This effect occurs for both, Series-I and Series-II.

Decreasing dimensions of the silica aggregates lead to increased filler-filler and filler-polymer interactions, which manifest themselves in a shift of the tan δ-curve towards higher temperature. The tan δ-peak for the compounds with constant silica loading shifts from -12 °C to -2 °C; see Table VI. It also shows that in particular the values of the loss modulus (G'') are decreasing with decreasing aggregate size, what suggests that the polymer chain movements are more restricted with decreasing aggregate size. At this moment however, a clear conclusion is difficult to draw about which interactions: filler-filler or filler-polymer, cause this effect because of the differences in the Payne effect for Series-I. However the adjustment of the silica loading in Series-II leads to similar Payne effects – similar filler-filler interactions; see FIG. 20. And in this case the tan δ-peak position is remaining relatively stable at a value of ca. -12 °C. Therefore, the position of tan δ-peak on the temperature axis or its width is more related to the filler-filler and less to the polymer-filler interactions.

The height of the tan δ-peak decreases when HDS are used both for the Series-I and Series-II, which means less hysteresis of the compounds. For the Series-II, the values of the loss modulus (G") are relatively constant and independent of the aggregate size; see

Table . However, the values of the storage modulus (G') measured for Series-II increase with decreasing aggregate size. Consequently, the variations in the tan δ maximum are here caused by differences in the sample stiffness. The filler-filler interactions measured for Series-II are similar, and therefore the changes in the tan δ maximum are caused by the filler-polymer interactions which increase the stiffness at temperatures close to the glass transition of the polymer.

TAN δ AT LOW TEMPERATURES: INDICATOR OF WET SKID RESISTANCE

Values of tan δ in the temperature region from 0° C to 20 °C are generally taken as indicator for the wet skid resistance of a tire tread. For the Series-I in which silica loading was kept constant, it can be seen in FIG. 23 that the tan δ-values for smaller aggregate size are higher than the values for the compounds containing larger aggregates. This effect is associated with filler-filler interaction as indicated before, as monitored in the Payne effect; FIG. 20. The higher the filler-filler interactions, the higher the values of the hysteresis, not only in the range of 0 - 20 °C, but also at higher temperatures.

When the silica loading is adjusted to obtain similar Shore A hardness an inverse dependence of the tan δ-values on the aggregate size is visible in the range of 0 - 20 °C. The equalization of the Shore A hardness leads to similar values of the Payne effect for the whole Series II. Therefore, the differences in the tan δ-values in this temperature range are caused entirely by changes in the filler-polymer interactions.

Polymer-filler interactions determine how well the polymer chains adsorb on the filler surface: physically via the entanglement of the polymer chains on the filler surface, chemically via covalent links between the filler surface and the polymer. Despite the fact that the silicas with the smallest aggregate sizes were used in lower concentration in Series-II, the adsorption of the polymer chains is still higher than for the silicas with larger aggregates used in higher concentrations. Increased adsorption of the polymer chains on the silica surface causes an

increase in the stiffness of the sample, demonstrated by a higher storage modulus for the silicas with smallest aggregates. The more polymer chains are adsorbed on the filler surface, the lower the hysteresis at both high and low temperatures.

As opposed to the case in which the silica loading was kept constant, in Series-II high values of the hysteresis between 0 - 20 °C are observed for the compounds containing silica with the largest aggregates, and are anticipated to correspond with higher values of the side force coefficient: see later.

TAN δ AT 60 °C: INDICATOR OF ROLLING RESISTANCE

Considering an average speed of a vehicle of 70 km/h and car wheel dimensions: 255/65/16, a typical frequency of deformation of the revolving tire is around 10 Hz. The hysteresis of the rubber compound causes an increase of the tire temperature to approx. 60 °C. The weight of the vehicle exerted on the tire is estimated to result in around 2 – 6 % tire tread deformation. Therefore, measuring tan δ values at 10 Hz, 2 % of dynamic strain and at 60 °C is a good indicator of rolling resistance. The lower the value of the tan δ under these conditions, the lower the predicted rolling resistance.

In FIG. 24 and FIG. 25, the silica types used in Series-I can be separated into two groups. The first have a low specific surface area and larger primary particles, which provide substantially lower values of tan δ at 60 °C. That is due to the good dispersibility of the larger particles (weaker filler-filler attraction forces) and less tendency to agglomerate. When each silica aggregate is surrounded by a rubber layer, there is less filler-filler friction and tendency to recombination of the filler network, thus lower hysteresis.

The second group of silicas includes SSA-195, SSA-200 and SSA-160, which give substantially higher values of tan δ at 60 °C caused by the higher specific surface areas and smaller aggregate

sizes. This leads to a more agglomerated filler in the polymer matrix manifested in the Payne effect and gives more inter-particle friction during dynamic deformation causing the energy loss. On the one hand, a decreased loading of the silicas SSA-200 (8 phr reduction) and SSA-195 (15 phr reduction) in order to adjust the hardness causes a substantial drop of the tan δ-values. On the other hand, increased loading of silicas with larger aggregates, SSA-80 (35 phr increase) and SSA-110 (15 phr increase), does not cause significant differences in comparison with constant loading of 80 phr. The dynamic properties of the pure elastomer are the governing factors for the composite material based on this elastomer. Reducing the amount of filler in the polymer matrix decreases the inter-particle friction by increasing the distance between the silica aggregates, which brings the hysteresis of the composite closer to the hysteresis of the pure elastomer.

Silica SSA-200 shows quite a different behavior compared to SSA-160 and SSA-195, as the tan δ value at 60 °C is lower than expected from its specific surface area. However, the reinforcing potential is still in the range of the highly reinforcing types of silica. This difference between SSA-200 and the other highly reinforcing types of silica might be explained by better dispersion of this silica type in comparison with the SSA-195, see FIG. 14. The dispersion level of SSA-200 is comparable with SSA-160 what explains similar values of the tan δ value at 60 °C for the two silica types.

LAT 100 SIDE FORCE COEFFICIENT: WET SKID RESISTANCE

Measurements were performed at different water temperatures; the results are shown in FIG. 26. Side force coefficient values increase with increasing surface area of silica. Increasing surface area of silica leads to higher values of tan δ between 0 and 20 °C, indicative of higher hysteresis. The ranking of the side force coefficient correlates roughly with the tan δ between 0 and 20 °C. Higher values of tan δ stand for more energy dissipation during wet skidding. Elastic material is

sliding over the surface of a relatively solid rough material: electro-corundum. Roughness of the disc surface causes micro-scale deformations on the wheel sample surface. On the one hand the elastic material which loses more energy during one deformation cycle will be characterized by higher values of the side force coefficient. One the other hand, elastic material with higher storage modulus (stiffer), will be also characterized by higher values of the side force coefficient, because its lower deformability in one deformation cycle leads to a higher force necessary to deform the rubber surface on micro-scale.

During skidding the surface of the rubber wheel undergoes small deformations trying to fill in the micro-cavities existing at the surface of the LAT-disc on which sliding is taking place. The load applied to the wheel, the average dimensions (depth and width) of the micro-cavities and the water film limit the degrees of micro-deformation. Since the wheel is moving with linear speed with respect to the sliding surface, the deformed compound which fills in the above mentioned cavities must be pushed back to its original position on the wheel.

Depending on the compound stiffness different wet skid scenarios can be envisaged. In the first case, the wheel is made out of very stiff compound which is not able to deform under the applied load, leading to extremely low wet skid resistance. In the second case, a wheel made out of soft rubber which deforms relatively easily, filling the micro-cavities until its dimensional limits – the wet skid resistance is much higher. However when less significant differences in the compound stiffness are considered, for instance when the load applied to the wheel exceeds the load needed to completely fill the micro-cavities for both the softer and stiffer compounds, the force necessary to push the stiffer compound back to its original position on the wheel is higher than the force needed to push back a softer compound. Hence, the wheel made out of the stiffer but still deformable compound will lead to a higher resistance during skidding. In such a case the side force coefficient correlates better with the values of the storage and loss moduli than with the

hysteresis. In Series-I, silica SSA-195 is characterized by the highest values of the side force coefficient and lowest loss modulus – high stiffness. In Series-II, the same silica is again characterized by the highest side force coefficient and highest storage modulus – high stiffness.

In Series-I, the SSA-80 provides the lowest values of the tan δ at 0 – 20 °C and its side force coefficient value is also the lowest among the other samples. However, in spite of the highest hysteresis in the range of 0 – 20 °C for the SSA-160, its side force coefficient values rank in the 3rd place. Regardless of the substantial differences in the hysteresis among the samples in Series-I, a correlation between the tan δ at 0 – 20 °C and the side force coefficients was not observed. This lack of correlation may be related to a minor contribution of the hysteresis during the measurements on the LAT-100 with the parameters selected.

Adjustment of the silica loading to equalize the hardness causes narrowing of the side force coefficient values range; see FIG. 27. The sample containing silica with the smallest aggregate size, SSA-195 is characterized by the highest values of the side force coefficient. Like for the other properties, the aggregate dimensions apparently have a dominant effect on the side force coefficient. Like in the case of Series-I, no apparent correlation between the tan δ at 0 – 20 °C and side force coefficient exists in this case.

Along with increasing temperature of the measurements, the values of the side force coefficient decrease for all compounds, because the elasticity of rubber increases. More elastic material loses less energy per deformation cycle, hence the side force coefficients decrease.

CONCLUSIONS

Five types of silica, differing in specific CTAB surface area and aggregate size, were tested in a passenger car tire compound. One of the silicas, SSA-200 is also characterized by different structure – its aggregates are larger while the specific surface are is similar to the SSA-195 type.

- The silica types with smaller aggregate dimensions and larger specific surface areas show a higher reinforcing effect, as illustrated by improved tensile properties. However, the dispersibility of these silicas is more difficult compared to the silica types with larger aggregates sizes. Compounds, in which SSA-195 was used, had superior tensile properties and the lowest loss modulus at lower temperatures. This silica type also resulted in the highest values of the side force coefficient, indicating best wet grip.
- Adjustment of the silica loading in order to obtain similar hardness of the cured compounds reverses the order of the dynamic curves. Silica with smallest aggregates is still superior regarding side force coefficient. However, the trend visible for constant silica loading has disappeared. This demonstrates that from the view point of wet skid resistance, smaller aggregates sizes of fillers are better, and that a higher aspect ratio of the fillers like in the case of SSA-200 type does not improve the wet skid resistance.
- Silicas with a larger aggregate sizes, SSA-80 and SSA-110 lead to low hysteresis at high temperatures, but the low reinforcing effect makes them also less appropriate as reinforcing filler for tire tread compounds.
- The dynamic properties of materials containing highly reinforcing silica can be further improved by using less filler, but the tensile properties will suffer in case of SBR/BR used as polymer matrix. Furthermore, good dispersion of the nano-sized aggregates is the key to obtain rubber composites with superior overall properties.

- With the selected measurement parameters for dynamic analysis and on the LAT-100, no correlation of the hysteresis at 0 – 20 °C with the side force coefficient was found for both series.

ACKNOWLEDGMENTS

This project was carried out in the framework of the innovation program ‘GO Gebundelde Innovatiekracht’, and funded by the ‘European Regional Development Fund’. The project partners Apollo Tyres Global R&D, Enschede, University of Twente (Tire-Road Consortium), Enschede, and Elastomer Research and Testing B.V., Deventer, all in the Netherlands, are gratefully acknowledged for their assistance.

REFERENCES

[1] M. J. Wang, RUBBER CHEM. TECHNOL., 71 (1998) 520.

[2] M. J. Wang, Kautsch. Gummi Kunstst., 60 (2007) 438.

[3] M. J. Wang, Kautsch. Gummi Kunstst., 61 (2008) 33.

[4] M. Heinz, K. A. Grosch, 167th Technical meeting of the Rubber Division ACS, May 16 -18 2005, San Antonio, Texas, USA.

[5] M. Heinz, J. Rubb. Res., 13 (2010) 91.

[6] K. R. Grosch, RUBBER CHEM. TECHNOL., 80 (2007) 379.

[7] C. J. Derham, R. Newell and P. McL. Swift, NR Technology, 19 (1988) 1.

[8] G. Heinrich, Kautsch. Gummi Kunstst., 45 (1992) 173.

[9] G. Heinrich, N. Rennar, H. Dumler, Kautsch. Gummi Kunstst., 49 (1996) 32.

[10] G. Heinrich, RUBBER CHEM. TECHNOL., 70 (1997) 1.

[11] M. Klüppel, G. Heinrich, RUBBER CHEM. TECHNOL., 73 (2000) 578.

[12] A. Müller, J. Schramm, M. Klüppel, Kautsch. Gummi Kunstst., 55 (2002) 432.

[13] A. le Gal, M. Klüppel, J. Phys. Condens. Matter, 20 (2008) 1.

[14] B. N. J. Persson, U. Tartaglino, E. Tosatti, O. Albohr, Kautsch. Gummi Kunstst., 57 (2004) 532.

[15] Y. Isono, T. Oyama, S. Kawahara, Adv. Tech. Mat. Proc. J. 5 (2003) 84.

[16] S. Uhrlandt, A. Blume 161th Technical meeting of the Rubber Division ACS, April 29 - May 1, 2002, Savannah, Georgia, USA.

[17] A. Blume, B. Freund, B. Schwaiger, M. Siray, S. Uhrlandt, EP0983966 A1 (2000), to Degussa-Hüls Aktiengesellschaft.

[18] H. D. Luginsland, 161th Technical meeting of the Rubber Division ACS, April 29 - May 1, 2002, Savannah, Georgia, USA.

[19] D. W. Schaefer, J. Appl. Crystallography 33 (2000) 587.

[20] S. Brunauer, P. H. Emmet, E. Teller, J. Am. Chem. Soc. 59 (1936) 2682.

[21] ASTM Standard D3765-02, "Test Method for Carbon Black— CTAB (Cetyltrimethylammoniumbromide) Surface Area"

[22] S. Uhrlandt, A. Blume, Rubber World 4 (2003) 43.

[23] A. Wehmeier, O. Stenzel, 7th Fall Rubber Colloquium DIK, November 8 – 11

2006, Hannover, Germany.

[24] Leaflet Hi-Sil EZ 200G, PPG Industries.

[25] S. L. Aggarwal, I. G. Hargis, R. A. Livigni, H. J. Fabris and L. F. Marker, "Advances in elastomers and rubber elasticity". Plenum Press (1986) 17.

[26] R. R. Rahalkar, RUBBER CHEM. TECHNOL., 62 (1989) 246.

[27] M. J. Wang, Kautsch. Gummi Kunstst., 61 (2008) 33.

[28] M. Heinz, J. Rubb. Res., 13 (2010) 91.

[29] K. R. Grosch, RUBBER CHEM. TECHNOL., 80 (2007) 379.

[30] R. Rauline, European Patent No. EP0501227B1, (1992), to Michelin Co.

[31] L. Guy, Ph. Cochet, Y. Bomal , S. Daudey, Kautsch. Gummi Kunstst., 63 (2009) 383.

[32] E. M. Dannenberg, RUBBER CHEM. TECHNOL., 48 (1975) 410.

[33] E. M. Dannenberg, Trans. Inst. Rubber Ind., 26 (1966) 42.

[34] M. Kaliske, G. Heinrich, RUBBER CHEM. TECHNOL., 72 (1999) 602.

[35] D. F. Jones, L. R. G. Treloar, J. Phys. D: Appl. Phys., 8 (1975) 1285.

[36] A. R. Payne, J. Appl. Polym. Sci., 6 (1962) 57.

FIGURE CAPTIONS

FIG. 1: Size distribution of silica aggregates for conventional and highly dispersible silica [18].

FIG. 2: Differences in silica structure for Zeosil 1200MP and 200MP.

FIG. 3: Principle of measurement on the LAT 100.

FIG. 4: Power profile for the different silica types during the first stage of mixing – Series I.

FIG. 5: Temperature profile during the first mixing stage – Series I.

FIG. 6: Power profile during the second mixing stage – Series I.

FIG. 7: Temperature profile during the second stage of mixing – Series I.

FIG. 8: Power profile during first mixing stage – Series II.

FIG. 9: Temperature profile during first mixing stage – Series II.

FIG. 10: Power profile during second mixing stage – Series II.

FIG. 11: Temperature profile during second mixing stage – Series II.

FIG. 12: Mooney viscosity versus CTAB specific surface area of different silica types.

FIG. 13: Mooney viscosity versus aggregate size of different silica types.

FIG. 14: Dispersion of the compounds Series I.

FIG. 15: Tensile strength in correlation with CTAB surface area.

FIG. 16: Tensile strength versus aggregate size.

FIG. 17: Elongation at break versus CTAB surface area.

FIG. 18: Elongation at break versus aggregate size.

FIG. 19: Payne effect versus CTAB surface area Series I and II.

FIG. 20: Payne effect versus aggregate size Series I and II.

FIG. 21: Shore A hardness in relation to aggregate size.

FIG. 22: DIN abrasion versus aggregate size.

FIG. 23: Tan δ – temperature dependence.

FIG. 24: Loss tangent at 60 °C versus CTAB specific surface area.

FIG. 25: Loss tangent at 60 °C versus aggregate size.

FIG. 26: Side force coefficient versus temperature – Series I.

FIG. 27: Side force coefficient versus temperature – Series II.

FIGURES

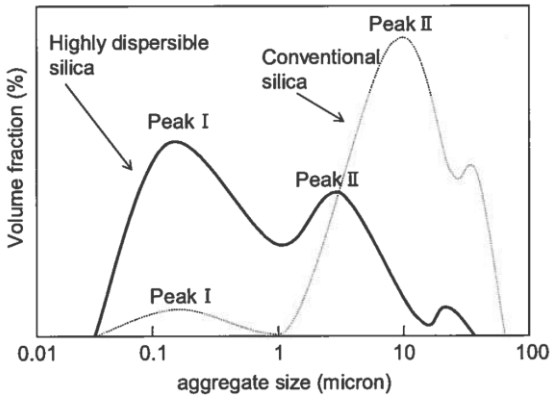

FIG. 1: Size distribution of silica aggregates for conventional and highly dispersible silica [18].

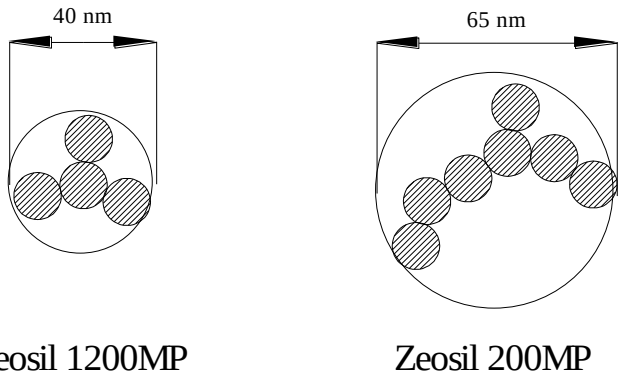

FIG. 2: Differences in silica structure for Zeosil 1200MP and 200MP.

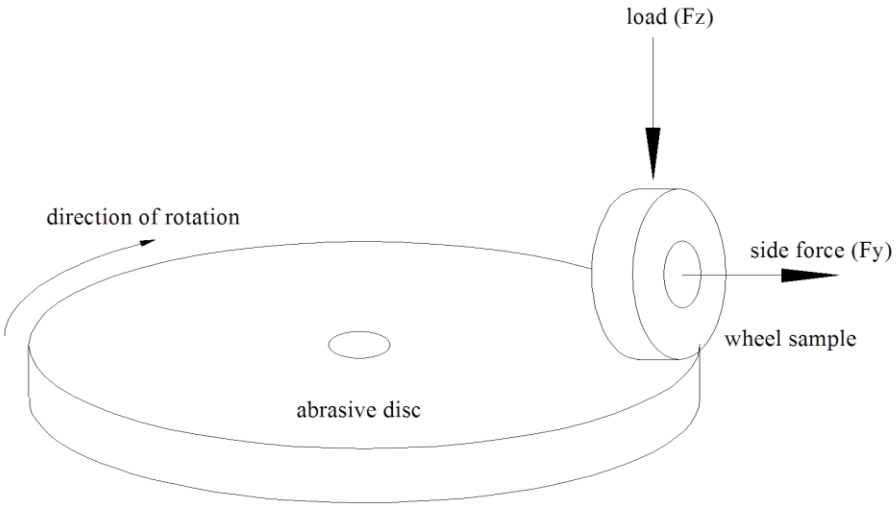

FIG. 3: Principle of measurement on the LAT 100.

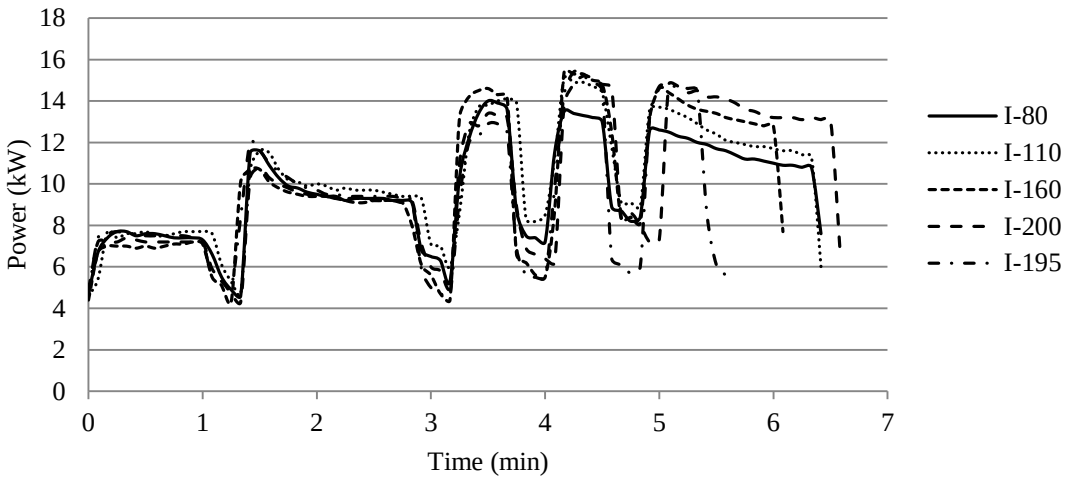

FIG. 4: Power profile for the different silica types during the first stage of mixing – Series I.

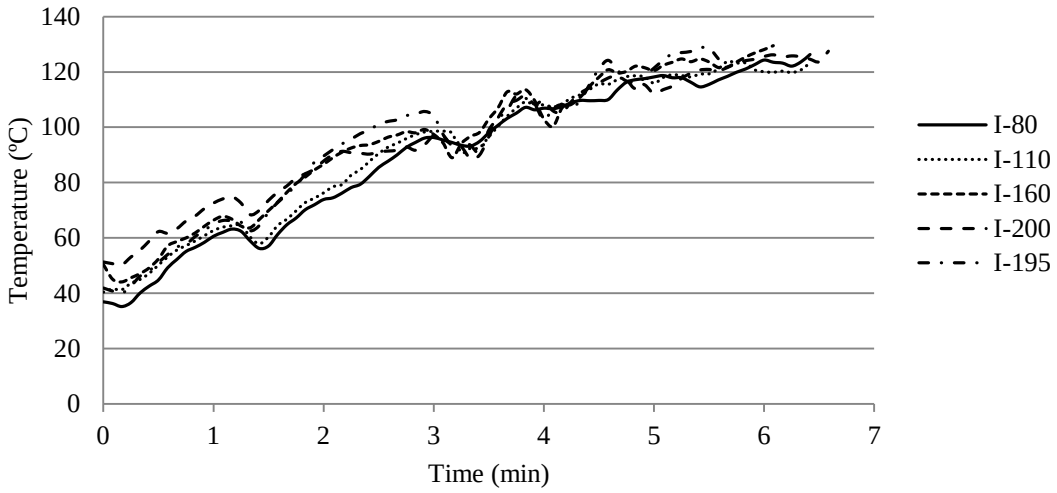

FIG. 5: Temperature profile during the first mixing stage – Series I.

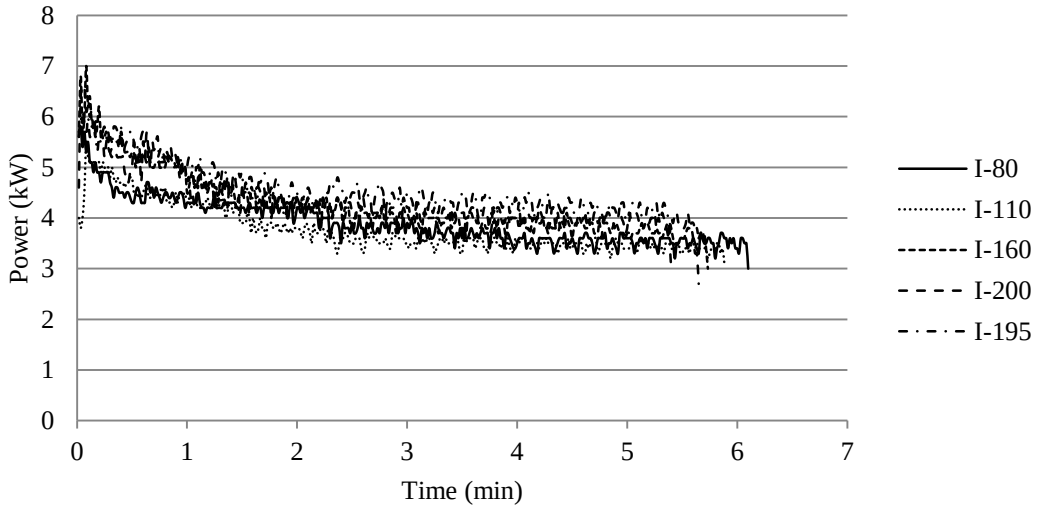

FIG. 6: Power profile during the second mixing stage – Series I.

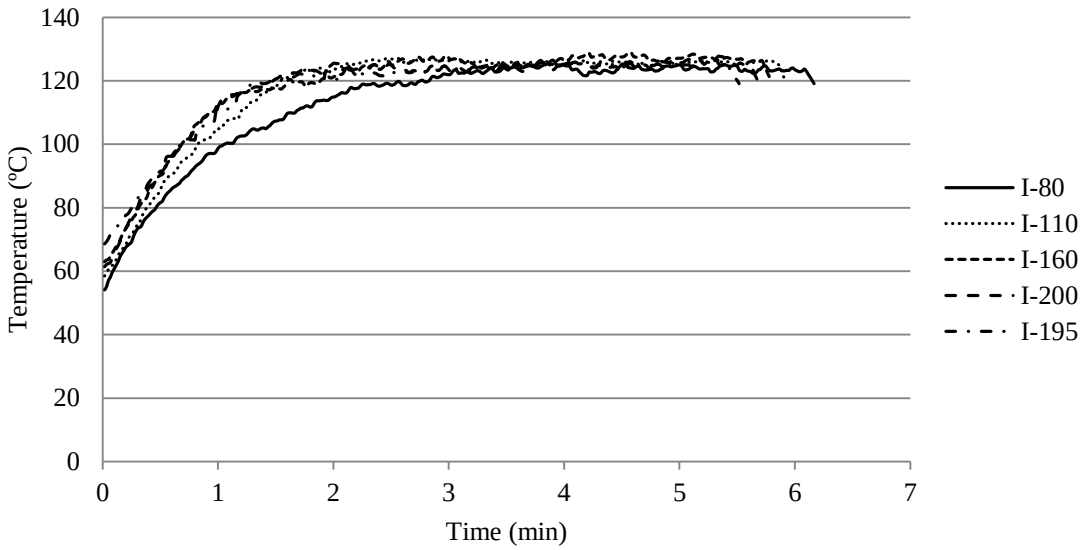

FIG. 7: Temperature profile during the second stage of mixing – Series I.

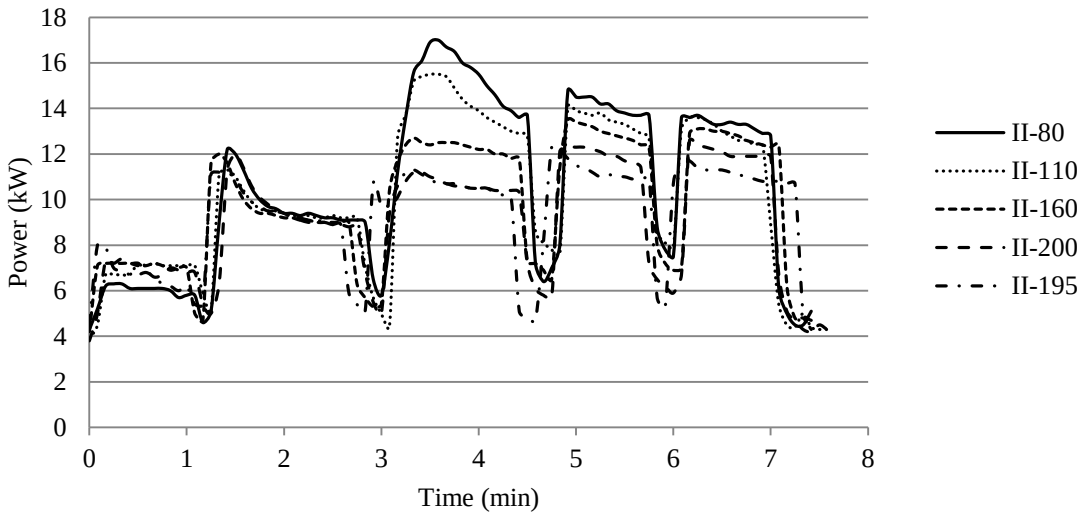

FIG. 8: Power profile during first mixing stage – Series II.

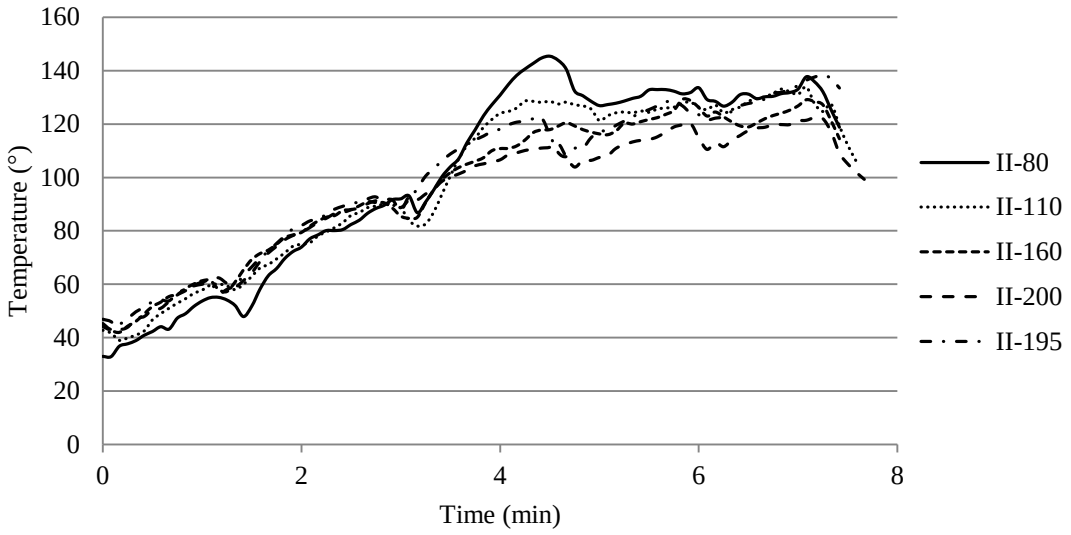

FIG. 9: Temperature profile during first mixing stage – Series II.

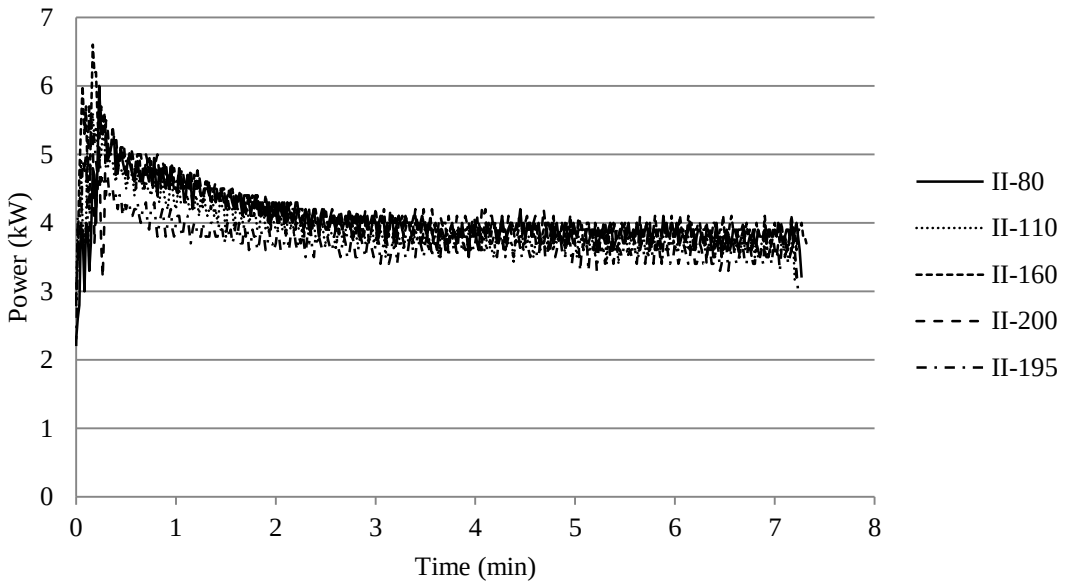

FIG. 10: Power profile during second mixing stage – Series II.

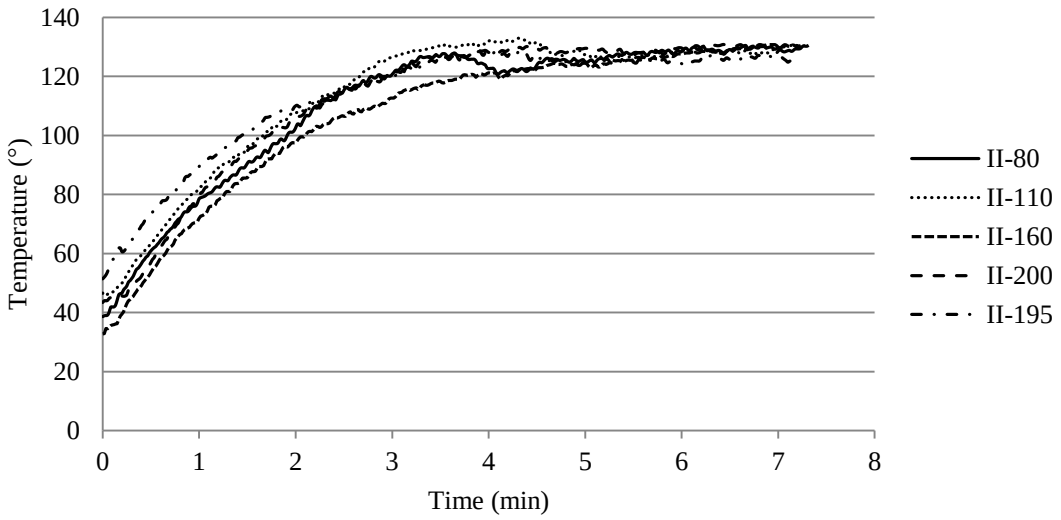

FIG. 11: Temperature profile during second mixing stage – Series II.

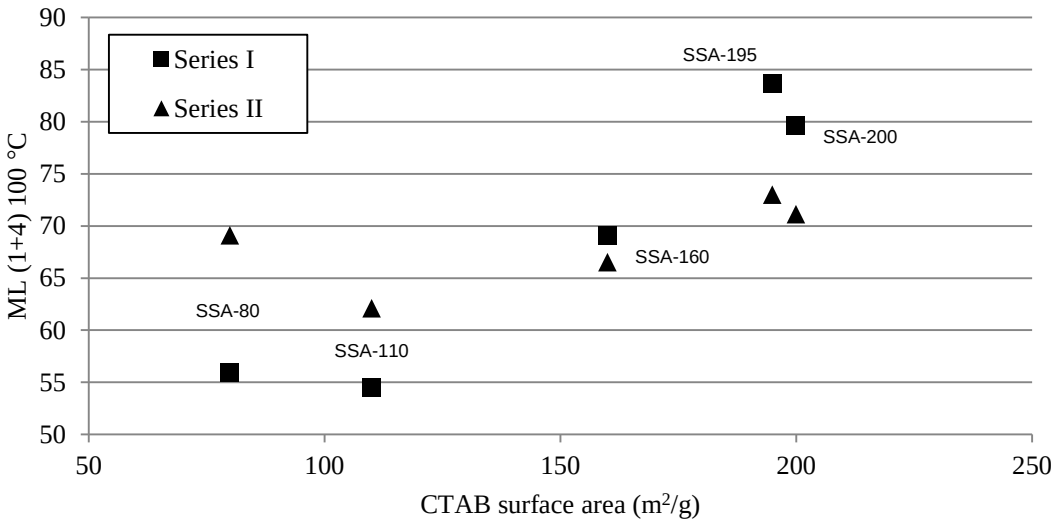

FIG. 12: Mooney viscosity versus CTAB specific surface area of different silica types.

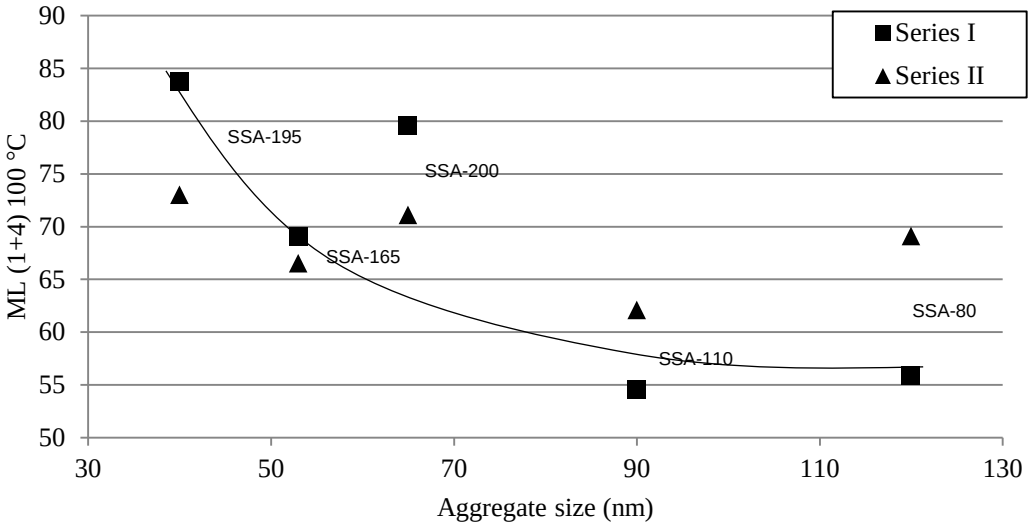

FIG. 13: Mooney viscosity versus aggregate size of different silica types.

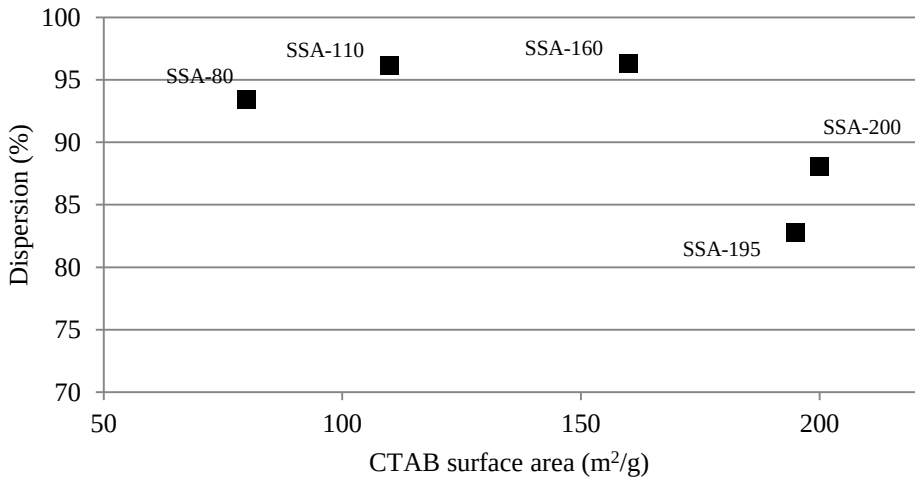

FIG. 14: Dispersion of the compounds Series I.

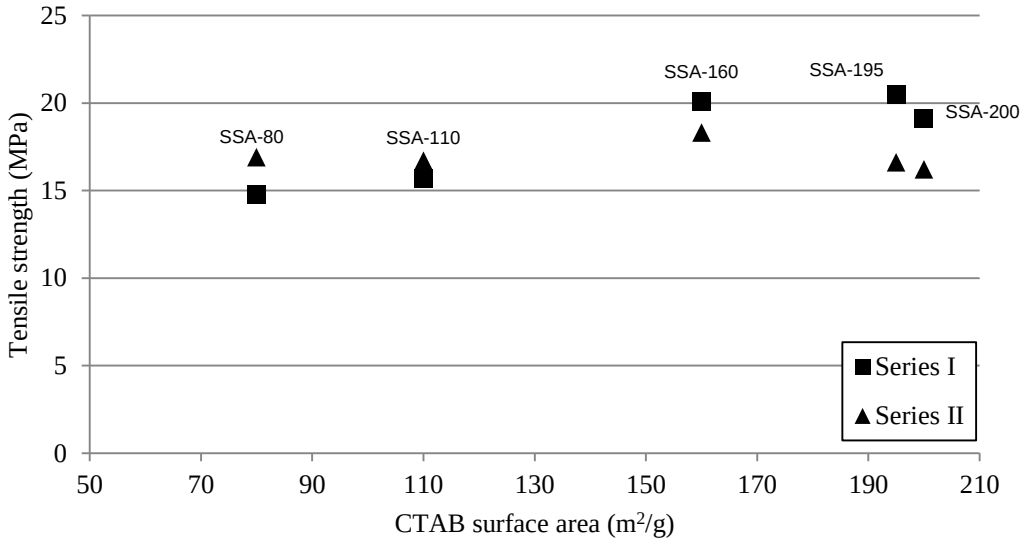

FIG. 15: Tensile strength in correlation with CTAB surface area.

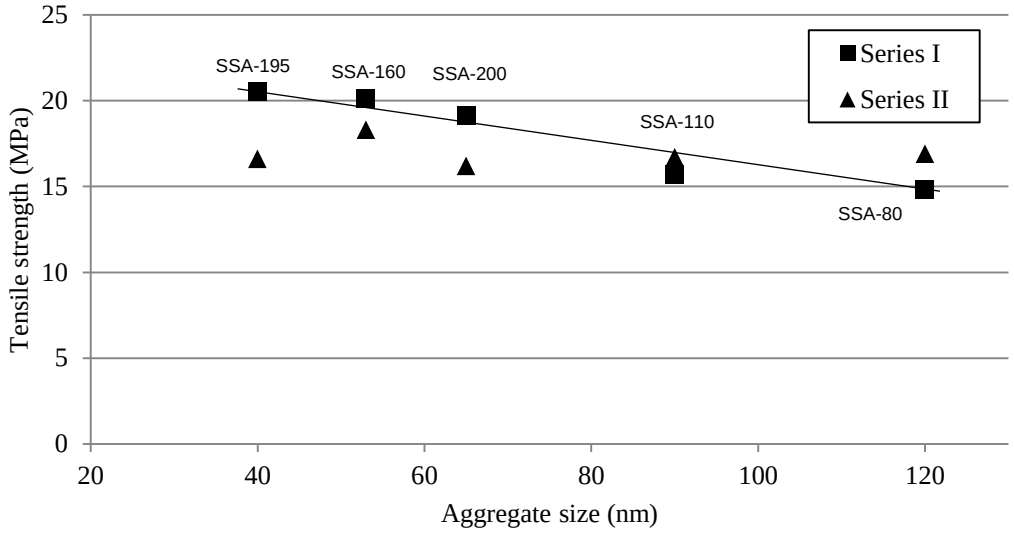

FIG. 16: Tensile strength versus aggregate size.

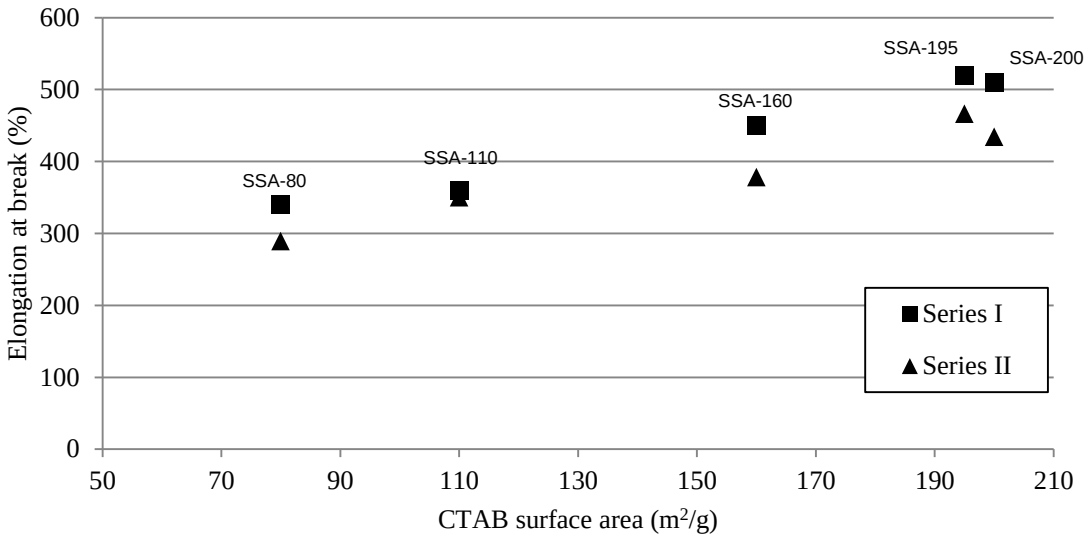

FIG. 17: Elongation at break versus CTAB surface area.

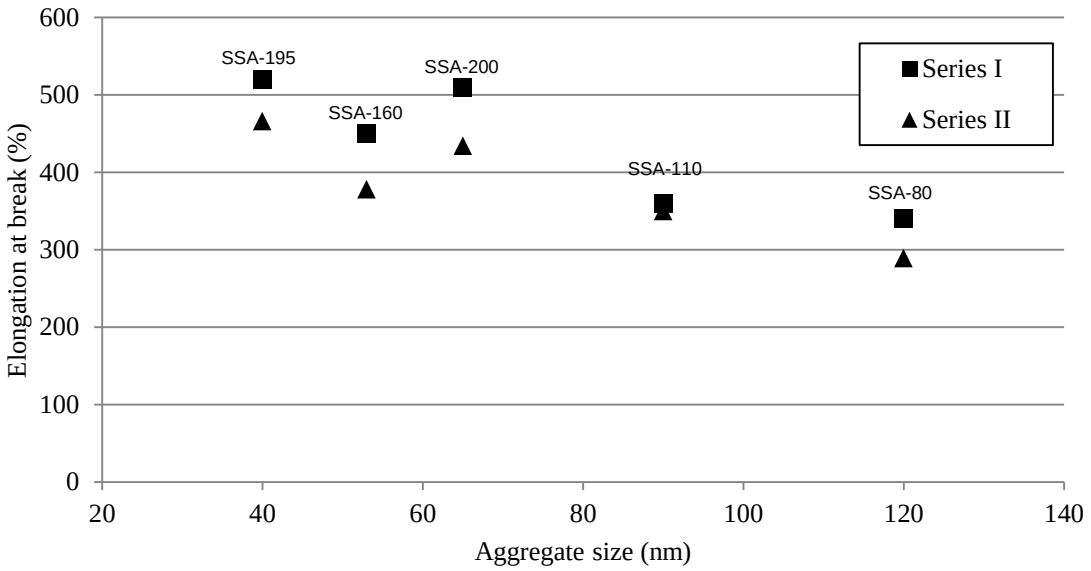

FIG. 18: Elongation at break versus aggregate size.

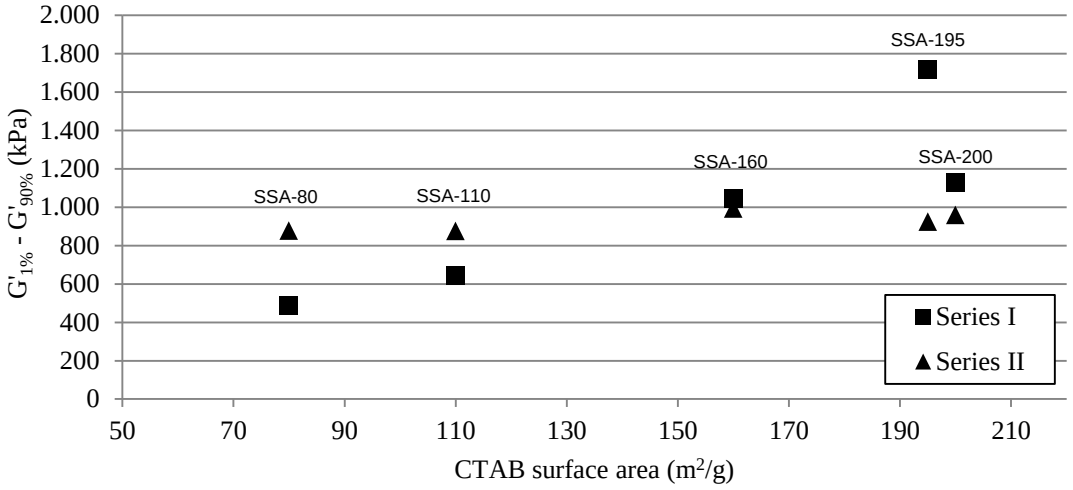

FIG. 19: Payne effect versus CTAB surface area Series I and II.

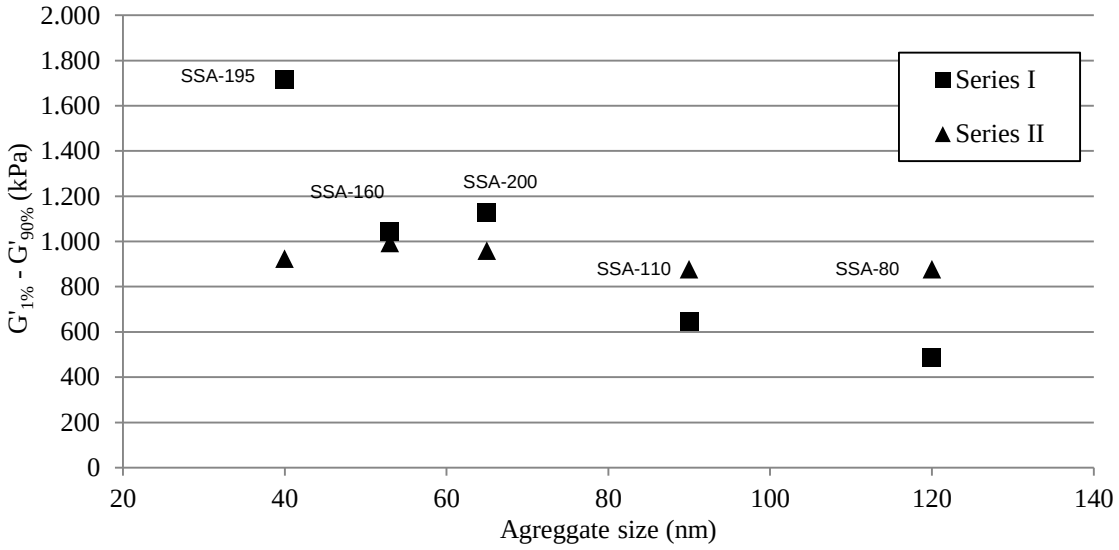

FIG. 20: Payne effect versus aggregate size Series I and II.

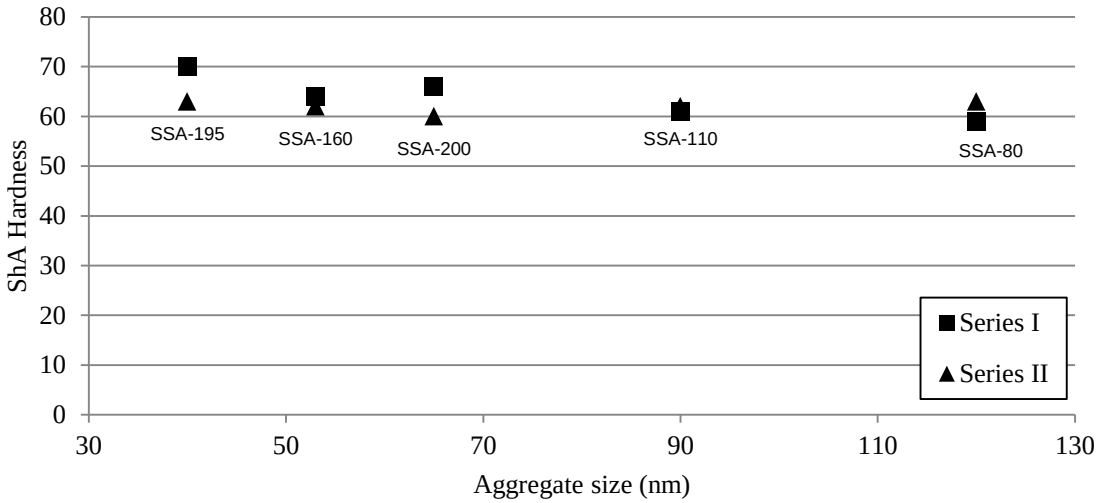

FIG. 21: Shore A hardness in relation to aggregate size.

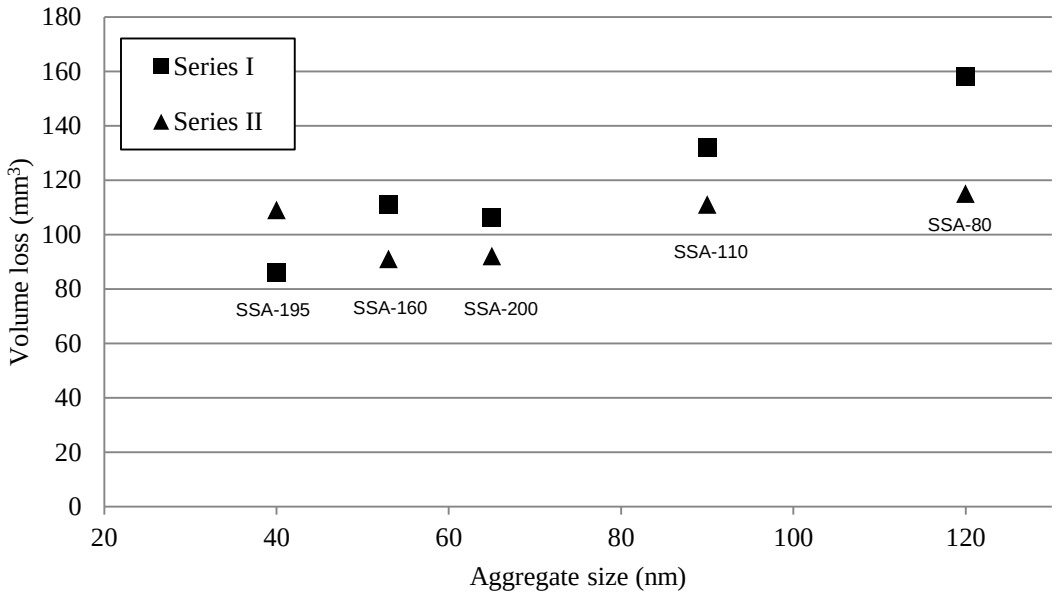

FIG. 22: DIN abrasion versus aggregate size.

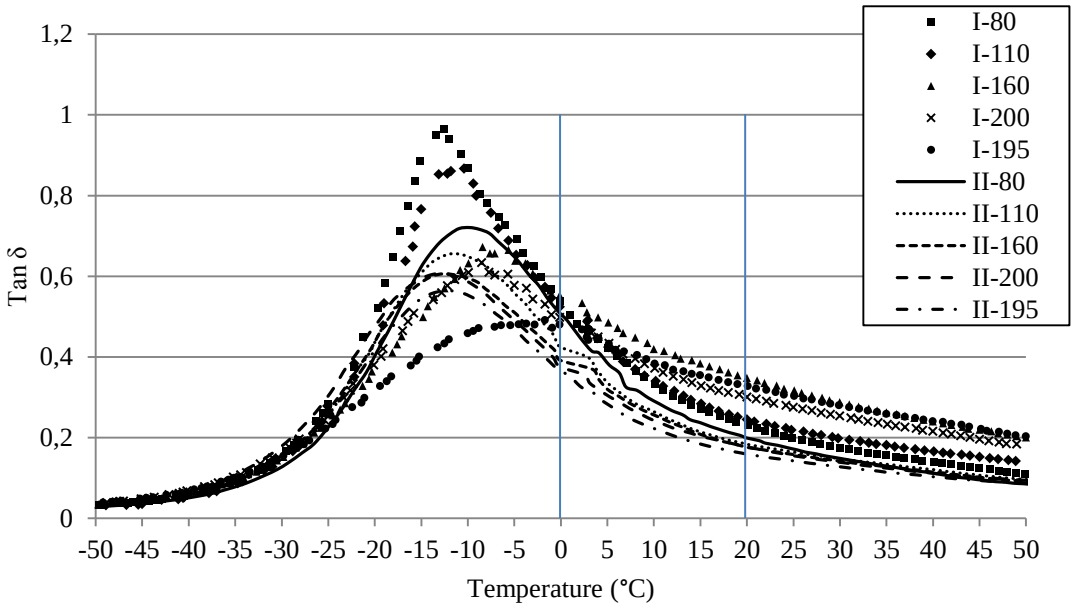

FIG. 23: Tan δ – temperature dependence.

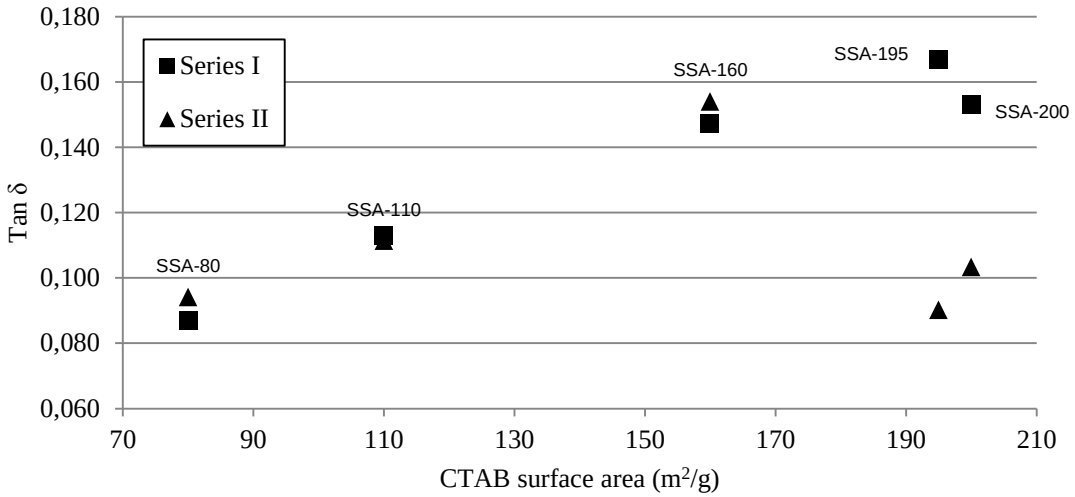

FIG. 24: Loss tangent at 60 °C versus CTAB specific surface area.

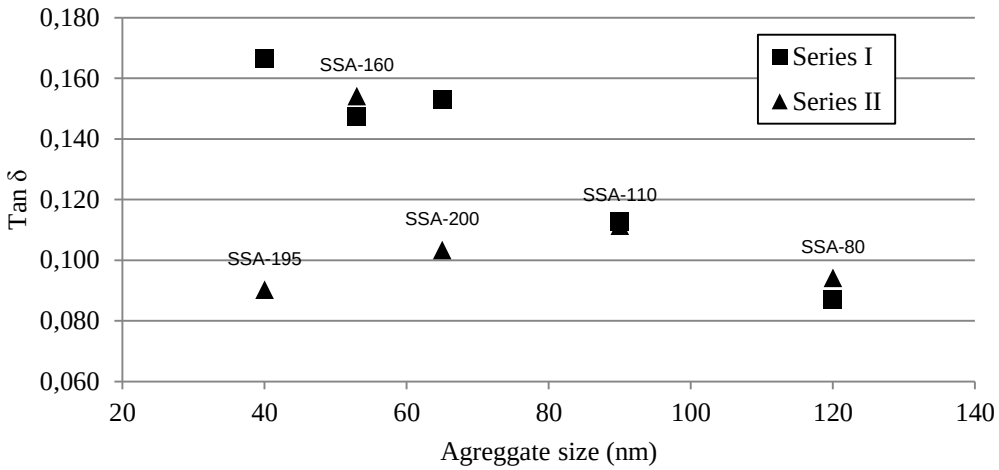

FIG. 25: Loss tangent at 60 °C versus aggregate size.

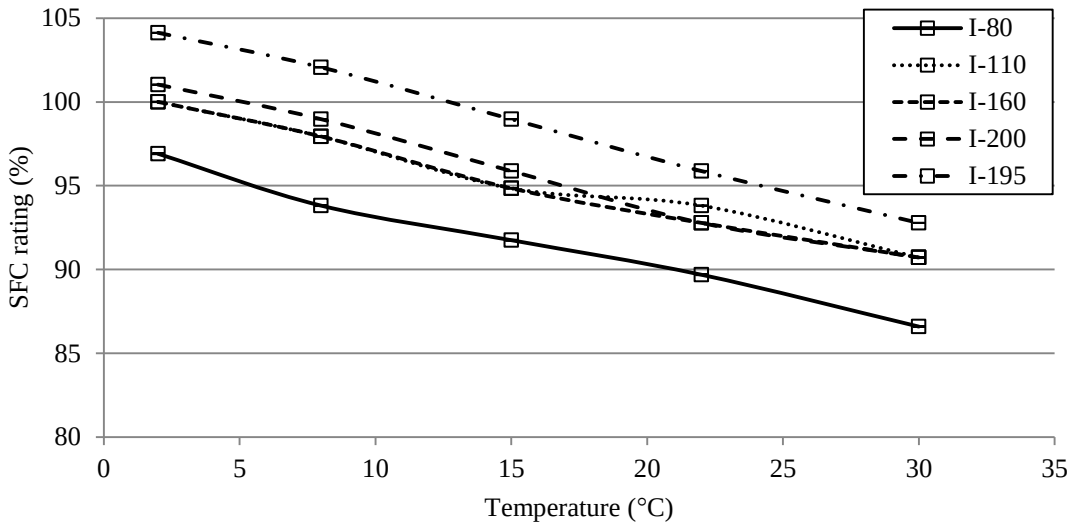

FIG. 26: Side force coefficient versus temperature – Series I.

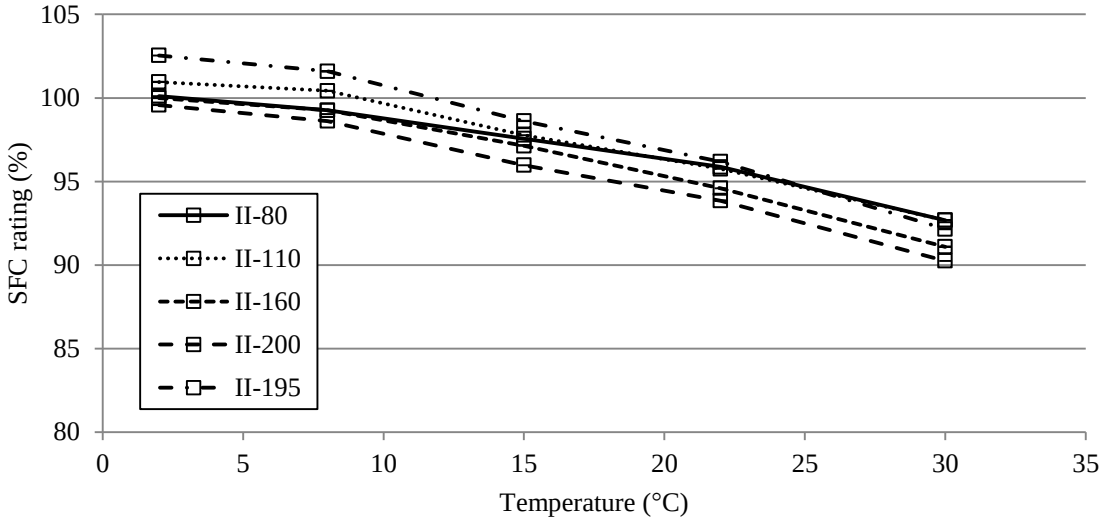

FIG. 27: Side force coefficient versus temperature – Series II.

TABLE CAPTIONS

Table I: Physical properties of the different silica types.
Table II: Ingredients specification.
Table III: Compound formulations – constant silica loading (Series I).
Table IV: Compound formulations – equal hardness (Series II).
Table V: Mixing procedure.
Table VI: Comparison of the storage and loss moduli for different silica types at the tan δ maximum.

Table I

Physical properties of the different silica types.

Silica characteristics					
Silica type	Zeosil 1085GR	Zeosil 1115MP	Zeosil 1165MP	Zeosil 200MP	Z HRS 1200MP
Silica code	SSA-80	SSA-110	SSA-160	SSA-200	SSA-195
BET surface area, m^2/g	90	115	165	215	200
CTAB surface area, m^2/g	80	110	160	200	195
Humidity, %	6.0	6.0	7.0	6.5	7.0
Mean diameter of aggregates, nm *	120	90	53	65	40
Diameter of elementary particles, nm **	-	25	20	10	15
Structure: Dioctyl adipate adsorption, ml/100 g	221	220	213	218	220

* Determined by X-ray disc centrifugation in water suspension after de-agglomeration in-situ using an ultrasonic probe

** Small-Angle X-ray scattering

Table II

Ingredients specification.

Ingredient	Specification	Supplier
S-SBR	Solution Styrene-Butadiene Rubber Buna VSL 5025-2 HM	Lanxess, Leverkusen, Germany
BR	High -cis Butadiene Rubber Europrene BR40	Eni Polimeri, Ravenna, Italy
TESPT	Bis-(triethoxysilylpropyl)tetrasulfide	Evonik GmbH, Essen, Germany
TDAE	Treated Distillate Aromatic Extract oil, VivaTec 500	Hansen & Rosenthal, Hamburg, Germany
Zinc oxide	Inorganic oxide	Sigma Aldrich, St. Louis, United States
Stearic acid	Organic acid	Sigma Aldrich, St. Louis, United States
6PPD	Antiozonant N-phenyl-N'-1,3-dimethylbutyl-p-phenylenediamine	Flexsys, Brussels, Belgium
TMQ	Antioxidant 2,2,4- trimethyl-l,2-di-hydroquinoline	Flexsys, Brussels, Belgium
Sulfur	Elemental sulfur, purified by sublimation	Sigma Aldrich, St. Louis, United States
TBBS	Accelerator N-tert-butylbenzothiazole-2-sulphenamide	Flexsys, Brussels, Belgium
DPG	Accelerator - diphenyl guanidine	Flexsys Brussels, Belgium

Table III

Compound formulations – constant silica loading (Series I).

	I-80	I-110	I-160	I-200	I-195
SBR Buna VSL 5025-2HM	103	103	103	103	103
Europrene BR40	25	25	25	25	25
SSA-80	80				
SSA-110		80			
SSA-160			80		
SSA-200				80	
SSA-195					80
TESPT	3,39	4,66	6,78	8,48	8,27
TDAE	5	5	5	5	5
Zinc oxide	2,5	2,5	2,5	2,5	2,5
Stearic acid	2,5	2,5	2,5	2,5	2,5
6PPD	2	2	2	2	2
TMQ	2	2	2	2	2
Sulphur	2,22	1,91	1,4	1,00	1,05
DPG	2	2	2	2	2
TBBS	1,7	1,7	1,7	1,7	1,7

Table IV

Compound formulations – equal hardness (Series II).

	II-80	II-110	II-160	II-200	II-195
SBR Buna VSL 5025-2HM	103	103	103	103	103
Europrene BR40	25	25	25	25	25
SSA-80	115				
SSA-110		95			
SSA-160			80		
SSA-200				72	
SSA-195					65
TESPT	5	5,5	6,8	7,6	6,7
TDAE	5	5	5	5	5
Zinc oxide RS	2,5	2,5	2,5	2,5	2,5
Stearic acid	2,5	2,5	2,5	2,5	2,5
6PPD	2	2	2	2	2
TMQ	2	2	2	2	2
Sulphur	1,8	1,7	1,4	1,2	1,42
DPG	2	2	2	2	2
TBBS	1,7	1,7	1,7	1,7	1,7

Table V

Mixing procedure.

Stage I	
Rotor speed: 75 RPM Initial temp.: 40 °C	
Timing,	Ingredient
Min. sec.	
0.0	Add polymers
1.0	Add ½ silica, ½ silane, ZnO + stearic acid
3.0	Add ½ silica, ½ silane, oil, TMQ, 6PPD
4.0	Sweep
6.30	Dump @ ~ 155 °C
Stage II	
Rotor speed: 90 RPM Initial temp.: 40 °C	
Timing,	Ingredient
Min. sec.	
0.0	Add I stage batch
6.30	Dump @ ~ 155 °C
Stage III	
Mixing in the curatives was performed on a two roll mill	

Table VI

Comparison of the storage and loss moduli for different silica types at the tan δ maximum.

Type	tan δ peak temp., °C	G', MPa	G'', MPa	tan δ
I-80	-12	32	31	0,96
I-110	-10	28	24	0,87
I-160	-6	29	19	0,66
I-200	-6	27	16	0,60
I-195	-2	33	16	0,49
II-80	-11	68	49	0,72
II-110	-11	69	46	0,66
II-160	-13	75	45	0,61
II-200	-14	79	48	0,60
II-195	-13	88	49	0,56